Nanoscale Advances

ROYAL SOCIETY OF CHEMISTRY

PAPER

View Article Online
View Journal | View Issue

Cite this: *Nanoscale Adv.*, 2022, **4**, 3073

Copper-doped carbon dots with enhanced Fenton reaction activity for rhodamine B degradation†

Zhiru Jin,‡[ac] Qiuying Li,‡[a] Peiduo Tang,‡[b] Ganfeng Li,[a] Li Liu,[a] Dong Chen,[b] Ji Wu,*[c] Zhihui Chai,*[b] Gang Huang *[b] and Xing Chen*[a]

The Fenton reaction has attracted extensive attention due to its potential to be a highly efficient and environmentally friendly wastewater treatment technology. Noble copper-doped carbon dots (CuCDs) are prepared through a simple one-step hydrothermal method with 3,4-dihydroxyhydrocinnamic acid, 2,2′-(ethylenedioxy)bis(ethylamine) and copper chloride, endowing the Fenton reaction with enhanced catalytic activity for rhodamine B (RhB) degradation. The effects of the concentration of CuCDs, temperature, pH, oxygen (O_2), metal ions and polymers on the catalytic activity of CuCDs are investigated. It is worth noting that electron transfer happening on the surface of CuCDs plays a vital role in the RhB degradation process. As evidenced by radical scavenger experiments and electron spin resonance (ESR) studies, CuCDs significantly boost the formation of hydroxyl radicals ($^{\bullet}OH$) and singlet oxygen ($^1O_2$), facilitating the Fenton reaction for RhB degradation. Due to the strong oxidation of ROS generated by the Fe^{2+} + H_2O_2 + CuCD system, RhB degradation may involve the cleavage of the chromophore aromatic ring and the de-ethylation process. Additionally, the toxicity of RhB degradation filtrates is assessed *in vitro* and *in vivo*. The as-prepared CuCDs may be promising catalytic agents for the enhancement of the Fenton reaction.

Received 30th April 2022
Accepted 7th June 2022

DOI: 10.1039/d2na00269h

rsc.li/nanoscale-advances

1. Introduction

To address a great threat to human health and the environment posed by wastewater, various methods and strategies have been applied for the removal of pollutants, such as adsorption,[1,2] biological degradation[3] and advanced oxidation.[4–6] Among them, Fenton oxidation is one of the green and effective advanced oxidation processes and plays an important role in the degradation of organic dyes.[7] The homogeneous Fenton reaction is composed of Fe^{2+}/H_2O_2, where the hydroxyl radical ($^{\bullet}OH$) generated by the reaction of Fe^{2+} with H_2O_2 attacks dye molecules and then converts them to low-toxicity or non-toxic small-molecular substances.[8] Several drawbacks, such as low utilization of H_2O_2, strict pH requirement and iron sludge induced by slow conversion of Fe^{3+}/Fe^{2+}, are not still addressed, limiting the development of the homogeneous Fenton reaction.[9,10] Considerable efforts have been devoted to enhancing the catalytic reactivity of the homogeneous Fenton reaction, *e.g.* fabrication of heterogeneous catalysts,[11] addition of reducing agents,[12,13] and varying experimental means (electro-Fenton, photo-Fenton).[14,15]

Carbon dots (CDs) are rapidly boosted in the aspect of synthesis and application owing to their small size, easy synthesis, excellent biocompatibility and unique optical and physical properties, thus being investigated in numerous potential applications, such as bioimaging,[16] drug delivery,[17] and sensing applications.[18–20] CDs can act as excellent potential catalysts thanks to their excellent intrinsic electron transfer characteristics.[21] CDs constructed with citric acid and thiourea are used as electron donors due to the high density of oxygen groups during the catalytic process. CDs prepared using *H. undatus* as the carbon source act as electron acceptors for catalytic reduction.[22]

Heteroatom-doping is an effective method to enhance the fluorescence intensity and the density of active sites.[23–25] Among heteroatom-doped CDs, inorganic doping affects the electrochemical properties of materials.[26,27] Copper-doped carbon dots (CuCDs), as inorganic doped CDs, have attracted considerable attention in the fields of drug delivery[28] and fluorescence probes.[29,30] Apart from those, CuCDs are employed as catalytic materials for the catalytic reaction of *p*-phenylenediamine[31] and *p*-nitrophenol.[32] Additionally, CuCDs prepared from ascorbic acid and Na_2[Cu(EDTA)] through pyrolysis possess reductive properties associated with the unsaturated valence and Cu^+,

[a]*School of Public Health, Guangxi Medical University, Nanning, 530021, China. E-mail: chenx63@163.com*

[b]*State Key Laboratory of Non-Food Biomass and Enzyme Technology, Guangxi Academy of Sciences, Nanning, 530007, China. E-mail: czh1716302002@163.com; wangyi.07@163.com*

[c]*Department of Ultrasonic Medicine, First Affiliated Hospital of Guangxi Medical University, Nanning, 530021, China. E-mail: gxnnwuji@126.com*

† Electronic supplementary information (ESI) available. See https://doi.org/10.1039/d2na00269h

‡ These authors contributed equally to this work.

differentiating from other CuCDs. Thus, CuCDs exhibit enhanced catalytic activity in the Fenton system,[33] which establishes that the reducing agents are conducive to the Fenton process.[12,13] However, it is unclear whether the other novel CuCDs tailored by altering the carbon source enhance the catalytic activity of the Fenton reaction.

In this work, CuCDs fabricated by a hydrothermal method were beneficial to accelerate RhB degradation in the Fenton process. The effects of the concentration of CuCDs, temperature, pH, O_2, metal ions and polymers on the catalytic reactivity of CuCDs were assessed. The reactive oxygen species (ROS) were identified by the scavenger test and ESR to elucidate the roles of ROS in the case of Fe^{2+} + H_2O_2 + CuCDs. On the basis of the results of liquid chromatography-mass spectrometry (LC-MS), a possible RhB degradation pathway was proposed. Furthermore, the toxicity of RhB degradation filtrates was investigated *in vitro* and *in vivo*.

2. Experimental section

2.1 Materials

RhB was bought from Tokyo Chemical Industry (TCI). 3,4-Dihydroxyhydrocinnamic acid (DHCA), 2,2′-(ethylenedioxy) bis(ethylamine) (EDA), iron(II) chloride tetrahydrate ($FeCl_2 \cdot 4H_2O$), iron(III) chloride hexahydrate ($FeCl_3 \cdot 6H_2O$), copper(II) chloride dihydrate ($CuCl_2 \cdot 2H_2O$) and calcium chloride dihydrate ($CaCl_2 \cdot 2H_2O$) were purchased from Energy Chemical Co. Ltd. Other chemicals were used without further purification. The 4T1 cell line and 293T cell line were obtained from the Cell Bank of Chinese Academy of Sciences. Kunming mice were obtained from Guangxi Medical University.

2.2 Preparation of CuCDs

364.3 mg (2 mmol) of DHCA and 341 mg (2 mmol) of $CuCl_2 \cdot 2H_2O$ were dissolved in 30 mL of deionized water and stirred for 5 min. Afterward, 0.584 mL of EDA was added and continuously stirred for 5 min at room temperature before transferring to an autoclave. After heating to 180 °C for 5 h, it was cooled to room temperature, centrifuged for 20 min (6000 rpm), and filtered three times with a 0.22 μm membrane. The filtrate was dialyzed against deionized water for 72 h (molecular weight cut-off (MWCO) = 500 D) before lyophilization, with changing the deionized water every 8 h during dialysis, and the resulting compound was denoted as CuCDs. Additionally, two other different proportions of CuCDs were prepared by a similar method but varying the Cu proportion (1 mmol of $CuCl_2 \cdot 2H_2O$ and 3 mmol of $CuCl_2 \cdot 2H_2O$), and the resulting compounds were denoted as 0.5CuCDs and 1.5CuCDs.

2.3 Characterization

Fourier-transform infrared (FT-IR) spectra were recorded on a Thermo Scientific Nicolet iS10 spectrometer. X-ray photoelectron spectroscopy (XPS) was performed using a Kratos Axis Ultra Dld. The UV-vis absorbance spectra were measured on an Agilent Cary 60 spectrophotometer. The crystal structure of the CuCDs was determined on an X-ray diffractometer (XRD) with a Cu–Kα radiation source operated at 40 kV, at a 10° min^{-1} scan rate, and 2θ from 0° to 80°. The morphology of the CuCDs was observed using a high-resolution transmission electron microscope (HRTEM) using a FEI Tecnai G2F20. Electron spin resonance (ESR) measurements were conducted using a Bruker A300. The copper content of the CuCDs was quantified by Thermo Fisher iCAP Qnova Series inductively coupled plasma mass spectrometry (ICP-MS). The elemental distribution of CuCDs was analyzed *via* scanning electron microscopy (SEM) with an energy dispersive spectrometer (EDS) on a Hitachi s-3400N. The fluorescence lifetime was measured on an Edinburgh Instruments FLS980. The quantum yield of CuCDs in deionized water was determined relative to a standard of quinine sulfate (a quantum yield of 0.54 in 0.1 M H_2SO_4). A series of CuCD solutions and quinine sulfate solution were prepared. The emission spectra of CuCDs or quinine sulfate solution between 400 nm and 650 nm were recorded, and the excitation wavelength was set at 350 nm. The integrated emission of solutions was plotted against the absorbance at 350 nm. The quantum yield of CuCDs (Φ_x) was calculated using the following formula:

$$\Phi_x = \Phi_{ST}\left(\frac{K_x}{K_{ST}}\right)\left(\frac{n_x}{n_{ST}}\right)^2$$

where Φ_{st} represents the quantum yield of quinine sulfate, K_x is the slope of CuCDs, K_{st} represents the slope of quinine sulfate, n_x represents the refractive index of the solvent for CuCDs, and n_{st} is the refractive index of 0.1 M H_2SO_4, the solution for quinine sulfate.

2.4 Evaluation of RhB degradation by accelerated Fenton reaction

1.5 mL of 1% H_2O_2 (V/V), 0.2 mL of 0.01 mol L^{-1} $FeSO_4$ solution, and 0.08 mL of 1 mg mL^{-1} RhB solution were added to deionized water in the absence and presence of CuCDs (10 mg mL^{-1}, 20 μL) within 90 min. The total volume of the mixture solution was 4 mL. Three sample solutions were prepared and 2.5 mL of sample solution was taken out for each measurement. The RhB degradation ratio was calculated using the following formula:

$$D\ (\%) = \left(1 - \frac{C}{C_0}\right) \times 100 = \left(1 - \frac{A}{A_0}\right) \times 100$$

where C and C_0 are the observed concentration at various time intervals and the initial concentration of RhB, and A and A_0 are the observed and the initial absorbance of the RhB solution at 550 nm, respectively.

The effects of temperature, pH, concentration of CuCDs, O_2, metal ions and polymers on RhB degradation by accelerated Fenton reaction were evaluated. For example, 1.5 mL of 1% H_2O_2 (V/V), 0.2 mL of $FeSO_4$ solution (0.01 mol L^{-1}), 0.08 mL of RhB solution (1 mg mL^{-1}) and 20 μL of CuCDs (10 mg mL^{-1}) were added to the deionized water and the solution volume was 6 mL. Three sample solutions were prepared and 2.5 mL of sample solution was taken out for each measurement. The above solutions were incubated at every temperature (25, 30, 40, 50, 60, 70, and 80 °C) for 5 min and then the absorbance of the

solution was recorded at 550 nm. Similarly, the effect of pH was tailored by altering pH *via* addition of HCl or NaOH solution under negligible total volume change. The effect of concentrations of CuCDs was evaluated under similar conditions except for addition of CuCDs in the range of 0–20 μL. To assess the effect of O_2, the reaction mixture (Fe^{2+} + H_2O_2 + CuCDs + RhB) was pumped with N_2 or O_2 gas for 30 min, while the original reaction mixture was used as the control. The effects of metal ions and polymers were evaluated through addition of NaCl, KCl, $FeCl_3$, $CuCl_2$, $CaCl_2$, $CdCl_2$, $AlCl_3$, $CrCl_3$, polyethylene glycol (PEG, M_n = 200), polyethyleneimine (PEI, M_n = 800) and poly(acrylic acid) (PAA, M_n = 3000).

To investigate the reproducibility of CuCDs, successive experiments were performed. Briefly, 0.09 mL of 1% H_2O_2 (V/V), 0.3 mL of $FeSO_4$ solution (0.01 mol L^{-1}), 0.12 mL of RhB (1 mg mL^{-1}), 0.03 mL of CuCDs (10 mg L^{-1}) and the deionized water were mixed and the total volume was 6 mL. The RhB absorbance was recorded after 30 min incubation. Then 0.09 mL of H_2O_2 and 0.12 mL of RhB were added to the above solution. After 30 min incubation, the RhB absorbance was also recorded. Similarly, 0.09 mL of H_2O_2 and 0.12 mL of RhB were added each time in the next three replicates and the RhB absorbance was recorded.

2.5 Toxicity assay *in vitro* and *in vivo*

After RhB degradation, the mixture was subjected to centrifugal separation for 20 min (6000 rpm). 0.4 g of NaCl, 0.01 g of KCl, 0.182 g of $Na_2HPO_4 \cdot 12H_2O$, and 0.012 g of KH_2PO_4 were dissolved in 50 mL of the RhB degradation filtrates followed by sterilization, and the resulting solution was denoted as the RhB degradation buffer solution.

2.5.1 MTT assay. 4T1 cells or 293T cells (10^4 cells per well) were seeded onto a 96-well plate for 24 h incubation. The cell culture medium was removed and the cells were incubated with various concentrations of the RhB degradation buffer solution for 24 h, whilst PBS was used as the control. Afterwards, 20 μL of MTT (5 mg mL^{-1}) in PBS and 180 μL of culture medium were added for another 4 h incubation. 100 μL of DMSO was added to each well and the absorbance was recorded using a Thermo Fisher Multiskan Go spectrophotometer at 570 nm.

2.5.2 CD measurements. 68 mg of bovine serum albumin (BSA) was dissolved in 100 mL of PBS solution. The BSA (the final concentration = 4×10^{-6} M) was incubated with the RhB degradation buffer solution. The CD spectra were recorded at room temperature under a N_2 atmosphere.

2.5.3 Hemolysis assay. Human red blood cells (HRBCs) were collected through centrifugal separation at 1500 rpm for 10 min and then were washed five times with PBS solution before dispersion in 4 mL of PBS solution. 500 μL of HRBCs were incubated with 500 μL of various RhB degradation filtrates for 3 h at 37 °C, while the deionized water and PBS were used as the positive control and negative control. The supernatant solution was measured using a UV-vis spectrometer at 540 nm after centrifugal separation at 1500 rpm for 10 min.

2.5.4 Hematoxylin–eosin (H&E) staining, hematology and blood biochemistry examinations *in vivo*. Kunming mice with a body weight of around 28 ± 3 g were randomly divided into 5 groups (n = 6 in each group) and were injected *via* the tail vein as follows: (a) PBS (control), (b) RhB degradation buffer solution (initial substrate RhB concentration of 40 mg L^{-1}), (c) the RhB concentration of 40 mg L^{-1} without degradation. The Kunming mice were injected once every two days for 21 days treatment and anesthetized with pentobarbital sodium for collection of the blood samples from the eyeball of mice. 150 μL of blood samples were assessed by hematology examinations and the rest of the blood samples were subjected to centrifugal separation for collecting the blood plasma for blood biochemistry examination. After the Kunming mice were sacrificed, the major organs (heart, liver, spleen, lung and kidney) were collected and the tissues were fixed in 4% paraformaldehyde and stained with H&E staining to assess cell damage of major organs.

2.6 Statistical methods

All the data in this work were calculated using SPSS 26.0 software and the results were expressed by the average value ± standard deviation (SD). The measurement data were compared by analysis of variance. A one-way analysis of variance (ANOVA) was performed when the variances were uniform. $P < 0.05$ was defined as statistically significant.

2.7 Live subject statement

All experiments were approved by the Ethics Committee of Guangxi Medical University and carried out in strict compliance with the relevant laws and institutional guidelines of Guangxi Medical University, Nanning, China.

3. Results and discussion

3.1 Characterization of CuCDs

The FT-IR spectra of CuCDs showed that the broad peaks in the range from 3826 to 2221 cm^{-1} were attributed mostly to carboxylic acid groups (–COOH) and hydroxyl groups (–OH), while the absorption band at 2881 cm^{-1} was characteristic of $–CH_2–CH_2–$ stretching vibrations (Fig. S1a†). The characteristic absorption peaks at 1554, 1450, 1396, 1101 and 1025 cm^{-1} were attributed to C=O, C–N, and C–OH stretching vibrations and symmetric C–O–C stretching.[34,35] The XPS results further confirmed chemical compositions of CuCDs. The chemical elements C, O and N co-existed on the surface of CuCDs as shown in the XPS survey spectrum of CuCDs (Fig. S1b†). The high-resolution XPS spectrum of C1s revealed three dominant peaks at 283.4, 284.9 and 286.7 eV, attributed to the presence of C–C/C=C groups, C–N bonds and C–O/C=O/C=N groups, respectively (Fig. S1c†).[36] The two fitted peaks at about 529.3 and 531 eV corresponded to C=O and OH, respectively (Fig. S1d†).[37,38] In the N1s spectrum, the peaks at 398.2 and 399.9 eV were assigned to C–N/O=C–N and NH_2 (Fig. S1e†).[39] Unfortunately, the Cu2p characteristic peaks were not observed in the XPS spectra due to the low amount of Cu in CuCDs (only 0.0584% Cu), which was confirmed by ICP-MS. EDS results showed that the elemental composition of the CuCD surface was C (66.23%), O (27.4%), and N (6.37%), and it was difficult

for EDS to show Cu deposition on the CuCD surface (Fig. S5 and Table S1†). Similarly, the Cu diffraction peak was not revealed in the XRD pattern (Fig. S1f†). A weak diffraction peak at $2\theta = 23.5°$ indicated that CuCDs generated an amorphous carbon structure, similar to the graphene sheet structure.[40] To assess the thermal stability of CuCDs, TGA was performed under N_2 or oxygen (O_2) (Fig. S1g†). CuCDs showed a rapid decomposition, about 60% of weight loss at 420 °C in a N_2 atmosphere, whereas CuCDs were completely destroyed after 546 °C in an O_2 atmosphere. CuCDs exhibited a negative zeta potential (-5.56 ± 1.46 mV) and a spherical shape with an average diameter of 2.6 nm and a lattice fringe distance of 0.14 nm in the HRTEM images (Fig. S1h and j†).

Two characteristic absorption peaks at 278 nm and 344 nm were observed in UV-vis spectra (Fig. S2a†). The peak centered at 278 nm was ascribed to the π–π* transitions of C=C in the conjugated double bond, and the other absorption peak at 344 nm was attributed to the n–π* transition of C=O.[41] The maximum emission wavelength was 443 nm when the excitation wavelength was set at 365 nm (Fig. S2a†). Additionally, CuCDs exhibited excitation-dependent fluorescence properties (Fig. S2b†). Interestingly, the fluorescence intensity of CuCDs was related to the concentrations of CuCDs and the maximum intensity was at 0.2 mg mL^{-1} (Fig. S2c†). No obvious fluorescence intensity changes were observed upon either the elevated temperature (Fig. S2d†) or the radiation of the UV lamp at 365 nm (Fig. S2e†). The fluorescence lifetime of CuCDs was calculated as 7.42 ns on the basis of the decay curve (Fig. S3a†) and the quantum yield was about 1.35% using quinine sulfate as a reference (Fig. S3b†).[42]

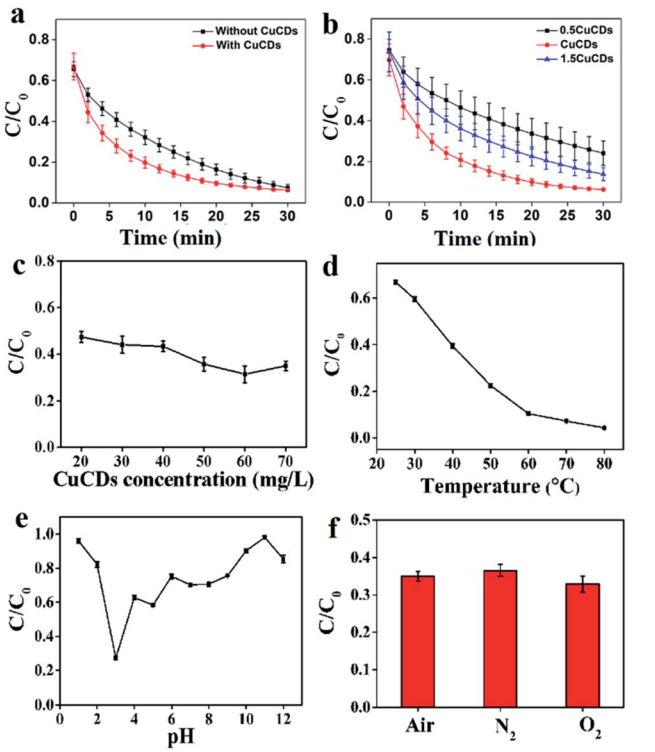

Fig. 1 The effects on RhB degradation upon the Fenton reaction: (a) the absence and presence of CuCDs; (b) different proportions of CuCDs; (c) CuCD concentrations; (d) temperatures, (e) pH values, and (f) the absence/presence of O_2.

3.2 Catalytic reactivity of CuCDs

The catalytic reactivity of CuCDs was assessed in terms of the RhB degradation evaluation. Fig. S3c† shows that (a) Fe^{2+}, (b) H_2O_2, (c) CuCDs, (d) Fe^{2+} + CuCDs, and (e) H_2O_2 + CuCDs removed less than 1% in 30 min, indicating that the contribution of these materials was negligible for RhB degradation. However, significant acceleration was achieved by addition of Fe^{2+} + H_2O_2 or Fe^{2+} + H_2O_2 + CuCDs. To further elucidate the influence of CuCDs on Fenton processes, RhB degradation processes with and without CuCDs were compared. It was established that the RhB degradation ratio was 80.99 ± 2.90% within 18 min and reached 92.52 ± 1.68% within 30 min (Fig. 1a). In the presence of CuCDs the RhB degradation ratio could reach 80.20 ± 2.73% using the Fe^{2+} + H_2O_2 system within 10 min (Fig. 1a), implying that the addition of CuCDs was conducive to enhancing the Fenton reaction rate. In addition, three different proportions of CuCDs were prepared through varying reacted Cu proportions and the corresponding Cu levels were 0.035%, 0.0584%, and 0.032% *via* ICP-MS. As depicted in Fig. 1b, the RhB degradation ratios were 53.53 ± 8.21%, 79.25 ± 3.17%, and 63.86 ± 5.97% during 10 min using various CuCDs. After 30 min, the RhB degradation ratios were 75.96 ± 6%, 93.83 ± 0.614%, and 86.26 ± 3.14%, illustrating that the CuCDs with 0.0584% Cu mass exhibited excellent RhB degradation performance among them and their RhB degradation performances were attributed to their composition. In this work, we chose the CuCDs with 0.0584% Cu mass as the main research object. The concentration of CuCDs was 20 mg L^{-1}, and the RhB degradation ratio was 52.62 ± 2.42% within 5 min. When the amount of CuCDs was 60 mg L^{-1}, the RhB degradation ratio increased to 68.62 ± 3.48%. Such a significant increase of degradation ratio was observed by varying concentrations of CuCDs (Fig. 1c), suggesting that CuCDs played an important role in RhB degradation.

3.3 Analysis of factors influencing the catalytic reactivity of CuCDs

The factors influencing the catalytic performance of CuCDs on RhB degradation were further evaluated, including temperature, pH, O_2, metal ions and polymers. As temperature was increased, the RhB degradation ratio gradually increased (Fig. 1d), indicating that the Fenton reaction was accelerated in the presence of CuCDs, which may be related to the fact that more ROS were yielded with increased temperature under protection of CuCDs, thus leading to more effective collision between ROS and RhB. As depicted in Fig. 1e, the Fe^{2+} + H_2O_2 + CuCD system showed the highest catalytic reactivity at pH = 3, because it tended to promote generation of ROS in an acidic environment.[43] To understand the role of O_2, either N_2 or O_2 was pumped into the Fe^{2+} + H_2O_2 + CuCD system. The result showed that it was unable to significantly tune the RhB degradation ratio (Fig. 1f).

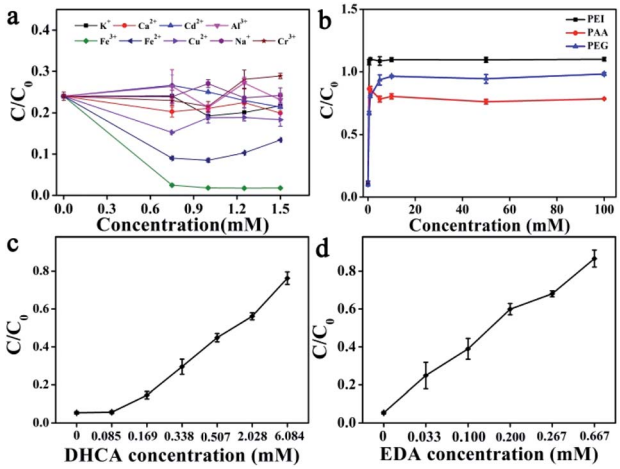

Fig. 2 The effects on RhB degradation in the case of Fe^{2+} + H_2O_2 + CuCDs: (a) metal ions; (b) polymers; substrate concentrations: (c) DHCA; (d) EDA.

The effects of metal ions and polymers on RhB degradation rates were investigated. Under the same experimental conditions, KCl, NaCl, $CaCl_2$, $CdCl_2$, $AlCl_3$ and $CrCl_3$ were respectively added to the Fe^{2+} + H_2O_2 + CuCD solution, which were unable to induce obvious changes in RhB degradation rates (Fig. 2a). Yet the RhB degradation ratio was increased upon addition of $FeCl_3$, $FeSO_4$ and $CuCl_2$ (Fig. 2a), which was responsible for the electron transfer. Generally, the fluorescence of CDs is quenched once electron transfer occurs. Hence, the fluorescence intensity of CuCDs was assessed upon the addition of various metal ions. There were no obvious changes in the fluorescence intensity of CuCDs upon addition of KCl, NaCl, $CaCl_2$, $CdCl_2$, $AlCl_3$ or $CrCl_3$ to the Fe^{2+} + H_2O_2 + CuCD system (Fig. S2f†). These results indicated that the electron transfer did not significantly occur among CuCDs and metallic salts (KCl, $CaCl_2$, $CdCl_2$, $AlCl_3$, NaCl, and $CrCl_3$) in the Fe^{2+} + H_2O_2 + CuCD system. However, the maximum fluorescence quenching of CuCDs occurred in the presence of Fe^{3+}, Fe^{2+} and Cu^{2+} (Fig. S2f†), which indicated that electron transfer occurred between CuCDs and metal ions (Fe^{3+}, Fe^{2+} and Cu^{2+}). Therefore, with the help of electron transfer, the RhB degradation ratio was improved after addition of $FeCl_3$, $FeSO_4$ and $CuCl_2$. It was worth mentioning that electron transfer played a vital role in the RhB degradation process. The effects of polymers with different electric charges on the RhB degradation rates were investigated. PEG, PEI, and PAA were used as a nonionic polymer, a cationic polymer and an anionic polymer in aqueous solution after hydrolysis. Similar to the aforementioned conclusion that the electron transfer was inhibited due to high medium concentration, the RhB degradation rates decreased in the presence of polymers because the polymers hindered the collision between $^{\bullet}OH$ and RhB. Interestingly, the RhB degradation ratio in the case of adding PAA was superior to those of addition of PEG or PEI, and it was lowest upon addition of PEI (Fig. 2b), which indicated that a nonionic polymer and a cationic polymer had greater effects on the RhB degradation ratio than an anionic polymer. In this work, the enhancement of RhB degradation with the help of CuCDs was attributable to the facilitation of electron transfer among Fe^{2+}, H_2O_2 and CuCDs in the Fenton process. Based on this, the anionic PAA was repelled by the CuCDs with negative charges because of electrostatic interactions, which did not entirely hinder the electron transfer among Fe^{2+}, H_2O_2, CuCDs and RhB. On the other hand, the cationic PEI was attracted to the surface of the CuCDs, impeding electron transfer. But for nonionic PEG, the RhB degradation ratio declined because the high concentration of PEG made the collision between $^{\bullet}OH$ and RhB inactive.

Besides, it was established that the reducing agents accelerated the Fenton reaction. In our work, the addition of CuCDs was conducive to enhancing the Fenton reaction rate, inspiring us to reveal whether the substrates (DHCA, EDA, and $CuCl_2$) or CuCDs acting as the reducing agents induced acceleration of the Fenton reaction in the case of Fe^{2+} + H_2O_2 + CuCDs. As displayed in Fig. 2c and d, the RhB degradation rates decreased with the increase of the concentrations of DHCA or EDA. The results implied that these substrates were unable to serve as the reducing agents to accelerate the Fenton reaction. As is well known, copper ions were able to accelerate the Fenton reaction. However, the CuCDs were dialyzed for 72 h and the water was changed every 8 h during the purification process to remove the copper ions. Previous studies indicated that the fluorescence of CDs was quenched by copper ions and recovered after addition of ethylenediaminetetraacetic acid (EDTA).[44] EDTA was able to readily form extremely stable chelating complexes with copper ions, resulting in that copper ions were away from the CuCDs. Thus the fluorescence of CuCDs was assessed in the absence/presence of EDTA (Fig. S3d†). As expected, the fluorescence of CuCDs was quenched by Cu^{2+} while it was recovered when EDTA was added. However, no obvious change in the fluorescence of CuCDs was observed after addition of EDTA, implying that a few copper ions were adsorbed on the surface, probably embedded inside the CuCDs. Thus the substrates did not serve as reducing agents to accelerate the Fenton reaction. Yet it was established that CDs with the hydroxyl groups exhibited reducing activity.[45] In this work, hydroxyl groups were introduced into CuCDs as evidenced by FT-IR and XPS, implying that the microstructure of CuCDs presumably served as the reducing agent to accelerate the Fenton reaction. In comparison to the RhB degradation based on CuCDs and Cu^{2+} with the same quantity of Cu, CuCDs offered higher catalytic activity (Fig. S3e†). Additionally, Table S2† summarizes the catalytic activity of conventional CDs toward other pollutants with various catalytic methods. Some CDs possessed inherent optical properties and were applied for the removal of RhB or methyl blue upon the photo-Fenton reaction. The Fenton reaction is commonly performed in a limited pH range. However, the addition of CDs didn't allow the Fenton reaction to get rid of the limitation of being performed in an acidic solution. In this work, CuCDs were able to help the Fenton reaction accelerate the degradation of RhB under neutral conditions without light irradiation, attributable to the role of CuCDs as co-catalysts. The degradation performance of CuCDs was superior to those of the other CDs.

3.4 Identification of ROS

Although $^{\bullet}OH$ was the major active species, $^1O_2$ and $^{\bullet}O_2^-$ were accompanied during the Fenton reaction. To further understand the roles of ROS in the catalytic process, various radical scavengers were utilized including isopropanol (IPA), 1,3-diphenylisobenzofuran (DPBF) and nitroblue tetrazolium (NBT) for $^{\bullet}OH$, $^1O_2$ and $^{\bullet}O_2^-$, respectively.[46,47] For the Fe^{2+} + H_2O_2 + CuCDs system, over 85% of RhB could be degraded after 32 min in the absence of IPA. With the addition of IPA to the Fe^{2+} + H_2O_2 + CuCD system, the RhB degradation ratio sharply decreased and became only 20.7 ± 0.04% after 32 min. This indicated that once $^{\bullet}OH$ was quenched by IPA, the catalytic activity of the Fe^{2+} + H_2O_2 + CuCDs system was dramatically reduced (Fig. 3a). The characteristic absorption peak of DPBF at 415 nm significantly decreased with time upon the addition of DPBF, indicating that $^1O_2$ was generated in the degradation system (Fig. 3b). Yet no obvious change in RhB degradation was observed despite the addition of NBT (Fig. 3c). These results indicated that $^{\bullet}OH$ and $^1O_2$ acted as the major ROS in the Fe^{2+} + H_2O_2 + CuCD system.

ESR, with 5,5-dimethyl-L-pyrroline-*N*-oxide (DMPO) and 4-amino-2,2,6,6-tetramethylpiperidine (TEMP) as the trapping agents for $^{\bullet}OH$, $^{\bullet}O_2^-$ and $^1O_2$, was performed to verify the species of ROS in the Fe^{2+} + H_2O_2 + CuCD system. The 1 : 2 : 2 : 1 four-wire signal characteristic peak was obtained in the absence of CuCDs, which corresponded to DMPO-$^{\bullet}OH$ (Fig. 3d). Upon the addition of CuCDs, the intensity of the DMPO-$^{\bullet}OH$ peak became stronger. The three-line ESR spectrum with equal intensities (1 : 1 : 1), corresponding to TEMP-$^1O_2$, was also slightly increased after addition of CuCDs (Fig. 3e). Nevertheless, the quadruple signal characteristic peak of DMPO-$^{\bullet}O_2^-$ with the ratio of 1 : 1 : 1 : 1 had a negligible change despite the addition of CuCDs (Fig. 3f). The ESR results demonstrated that $^{\bullet}OH$ mainly contributed to RhB degradation, $^1O_2$ was secondary and $^{\bullet}O_2^-$ was the weakest among them, which were consistent with the results of the scavenger test. It was reported that the $^{\bullet}O_2^-$ derived from the $^{\bullet}OH$[48] and $^1O_2$ was produced from $^{\bullet}O_2^-$.[49] Negligible changes of $^{\bullet}O_2^-$ were observed, along with subsequent upregulation of $^1O_2$ levels, suggesting that CuCDs could directly or indirectly induce a higher level of $^1O_2$. The speculation was shown as below:

$$Fe^{2+} + H_2O_2 \xrightarrow{CuCDs} Fe^{3+} + {\bullet}OH + OH^- \quad (1)$$

$$\cdot OH \xrightarrow{CuCDs} \cdot O_2^- \xrightarrow{CuCDs} {}^1O_2 \quad (2)$$

(or $\cdot OH \xrightarrow{CuCDs} {}^1O_2$)

3.5 Optimization of the H_2O_2/Fe^{2+} molar ratio and degradation kinetics

With increasing the H_2O_2/Fe^{2+} molar ratio, the RhB degradation ratio was initially increased and then slightly decreased for the Fe^{2+} + H_2O_2 + CuCD system, in which the optimum H_2O_2/Fe^{2+} molar ratio was approximately 10 : 1 in the RhB concentration range from 20 to 40 mg L^{-1} (Fig. 4a). Additionally, the catalytic activity for the Fe^{2+} + H_2O_2 + CuCD system was further evaluated at different RhB concentrations (Fig. 4b). The degradation ratios were over 94.32 ± 1.58% in the RhB concentration range from 10 to 50 mg L^{-1}, suggesting that RhB was almost destructed by ROS. Yet at a higher RhB concentration (>50 mg L^{-1}), the degradation ratio slightly declined, only 90.29 ± 0.26% despite prolonging incubation for another 2 h, which demonstrated that a few RhB molecules were not completely degraded. The Langmuir–Hinshelwood model was adopted to quantitatively analyze pseudo-first-order kinetics: $\ln(C_0/C_t) = kt$.[50] The ratio constant k could be calculated from the plot of $-\ln(C_0/C_t)$ *versus* t within 60 min and the k values were 0.1481, 0.1322, 0.06233, 0.04568, 0.03915, and 0.0238 min^{-1}, corresponding to RhB concentrations of 10, 20, 30, 40, 50, and 60 mg L^{-1}. Regression coefficient (R^2) values of the fitted lines were 0.8958, 0.9605, 0.9784, 0.9161, 0.9209, and 0.9435, respectively (Fig. 4c). The results showed that the overall trend of degradation efficiency declined as the RhB concentration increased.

3.6 Fine chemical treatment and the possible degradation mechanism

Since RhB was decomposed, flocculent precipitation occurred. The mixture solution was separated through centrifugation. The amounts of Fe and Cu in either the filtrates or the aggregates were quantified by ICP-MS. The Fe ratio was denoted as the amounts of metal in the filtrates to those in the aggregates. The Cu ratio was calculated by the same method. The results showed that the Fe ratio decreased as the RhB concentration

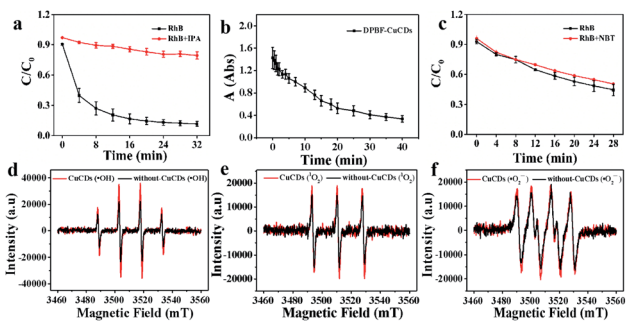

Fig. 3 The radical scavenger experiments: (a) IPA; (c) NBT probe as a radical scavenger; (b) UV-vis absorption of DPBF at different times in the presence of CuCDs in solution; ESR signals generated by the Fenton reagent with or without CuCDs in solutions: (d) $^{\bullet}OH$ radicals; (e) $^1O_2$; (f) $^{\bullet}O_2^-$ radicals.

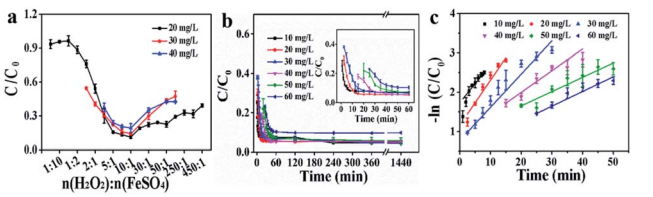

Fig. 4 (a) The effect of the ratio of H_2O_2 to $FeSO_4$ on RhB degradation; (b) the effect of substrate RhB concentrations on degradation; (c) the $-\ln(C/C_0)$ *vs.* time curves of RhB degradation.

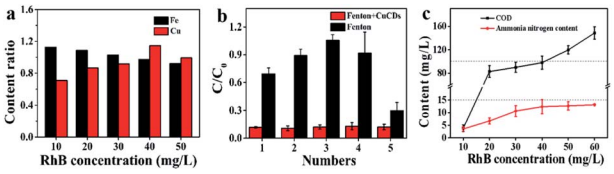

Fig. 5 (a) The liquid-to-solid ratio of Fe and Cu contents under different substrate RhB concentrations; (b) the recycles of H_2O_2 and RhB on degradation; (c) COD and ammonia nitrogen content of the degraded solution.

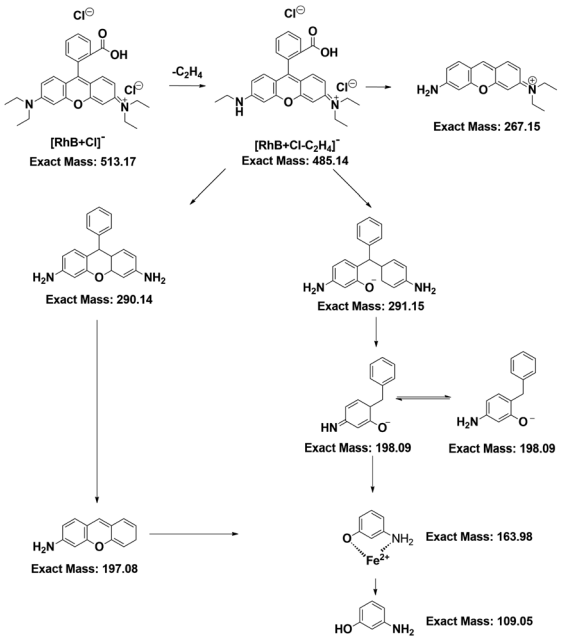

Fig. 6 RhB degradation pathway in the case of Fe^{2+} + H_2O_2 + CuCDs.

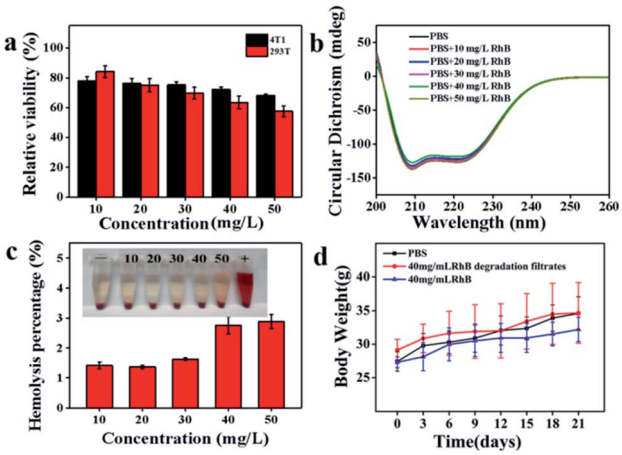

Fig. 7 (a) The mixture incubated with 4T1 and 293T cells in the different concentrations of RhB degradation filtrates; (b) the effects of the RhB degradation filtrates on the secondary structure of BSA; (c) hemolysis assay in the different RhB degradation filtrates; (d) the effect of different concentrations of RhB on body weight.

increased (Fig. 5a), suggesting that the Fenton reaction needed more Fe^{2+} to achieve RhB degradation, leading to the abundant formation of iron sludge. Yet the Cu ratios slightly increased (Fig. 5a). Perhaps CuCDs could participate in the Fenton reaction to yield more copper ions and fewer unreactive CuCDs were adsorbed onto the surface of the sludge, resulting in an increased Cu ratio. Inspired by the above results, we further assessed whether the addition of H_2O_2 and RhB alone to the filtrate could continue degrading RhB. It was noticed that the RhB degradation ratios remained above 85% in the Fe^{2+} + H_2O_2 + CuCD system for five successive experiments (Fig. 5b), which was superior to the RhB degradation rates in the Fe^{2+} + H_2O_2 system, implying that the RhB filtrate was able to be reused to degrade RhB as long as replenishing H_2O_2. However, the RhB solutions with various concentrations from 10 to 60 mg L^{-1} were decomposed in the case of Fe^{2+} + H_2O_2 + CuCDs. The results showed that the values of chemical oxygen demand (COD) and ammonia nitrogen tended to be high with increasing substrate RhB concentrations, suggesting that more RhB molecules were not decomposed with increasing RhB concentrations. When the substrate RhB concentration was at

Table 1 Blood routine examination of mice after intravenous treatment with the RhB degradation filtrate (substrate RhB concentration = 40 mg L^{-1}) or RhB solution (40 mg L^{-1}) for 21 days[a]

Blood routine index	Control group	RhB degradation filtrate	*P**	RhB solution	*P**
WBC (10^9 L^{-1})	2.53 ± 0.79	2.16 ± 0.73	0.394	2.28 ± 0.64	0.002
RBC (10^{12} L^{-1})	8.97 ± 1.03	8.15 ± 0.47	0.070	7.15 ± 0.54	0.001
HGB (g L^{-1})	118.83 ± 13.35	146.16 ± 25.93	0.083	103.67 ± 2.50	0.009
HCT (%)	39.38 ± 3.67	35.66 ± 2.61	0.048	33.80 ± 2.57	0.006
MCV (fL)	43.95 ± 1.32	43.80 ± 1.86	0.883	42.48 ± 1.93	0.163
MCH (pg)	13.13 ± 0.43	13.36 ± 0.56	0.480	14.88 ± 0.88	0.000
MCHC (g L^{-1})	310.00 ± 4.86	306.83 ± 5.95	0.333	306.00 ± 5.58	0.226
PLT (10^9 L^{-1})	731.5 ± 104.1	722.8 ± 120.4	0.879	715.00 ± 53.12	0.772
RDW (%)	15.68 ± 0.56	15.55 ± 0.93	0.813	16.30 ± 1.25	0.283
MPV (fL)	5.11 ± 0.17	5.50 ± 0.39	0.092	5.18 ± 0.47	0.758
RDW (%)	15.68 ± 0.56	15.55 ± 0.93	0.211	16.30 ± 1.25	0.437
PCT (%)	0.45 ± 0.05	0.40 ± 0.08	0.136	0.44 ± 0.06	0.713

[a] **P*, compared with the control groups.

40 mg L^{-1}, the values of COD and ammonia nitrogen were 97.93 ± 11.11 mg L^{-1} and 12.36 ± 2.76 mg L^{-1}, respectively (Fig. 5c).

With the help of LC-MS, more detailed information about intermediates was obtained. The RhB degradation filtrates were measured as depicted in Fig. S4a-f.† The major mass peaks appeared at *m*/*z* 487, 293, 197, 160 and 109, which could be assigned to $C_{26}H_{27}Cl_2N_2O_3^-$, $C_{19}H_{19}N_2O^-$, $C_{13}H_{12}NO^-$, $C_6H_5FeNO^-$ and $C_6H_6NO^-$, respectively. As the RhB concentration increased, the intensities of these two peaks at 487 and 293 increased, indicating that the RhB degradation underwent a de-ethylation process. Based on the results of LC-MS, a possible RhB degradation pathway was proposed (Fig. 6). The strong oxidation of ROS caused the cleavage of the chromophore aromatic ring and the de-ethylation process from the aromatic ring with a hypsochromic shift. Then, RhB was converted into low-toxicity even non-toxic compounds.

3.7 Toxicity of RhB degradation filtrates *in vitro* and *in vivo*

The toxicity of the RhB degradation filtrates was investigated after centrifugal separation using the MTT assay. NaCl, KCl, Na_2HPO_4 and KH_2PO_4 were dissolved in the RhB degradation filtrates and the mixture was incubated with 4T1 or 293T cells for 24 h. As depicted in Fig. 7a, the degradation filtrate corresponding to a substrate RhB concentration of 10 mg L^{-1} showed low cytotoxicity toward cells (4T1 and 293T) and the cell viabilities were 78.06 ± 2.64% and 84.19 ± 3.95%, respectively. The decrease in cell viability showed that the cell viability depended on the substrate RhB concentration. Additionally, the effect of the RhB degradation filtrates on the secondary structure of BSA was investigated. However, no obvious secondary structure difference in BSA was observed at 209 nm and 222 nm (Fig. 7b), suggesting that the RhB degradation filtrates had weak effects on the α-helix structure of BSA. A hemolysis assay was performed to further evaluate the blood biocompatibility *in vitro*. The hemolysis percentages were 1.41 ± 0.12%, 1.37 ± 0.05%, 1.63 ± 0.03%, 2.75 ± 0.29%, and 2.88 ± 0.23%, corresponding to the substrate RhB concentrations in the range of 10–50 mg L^{-1} (Fig. 7c), indicating that the RhB degradation filtrates had negligible hemolytic activity.

Hematology, blood biochemistry and histopathology examinations were performed to evaluate the biocompatibility of RhB degradation filtrates *in vivo*. The Kunming mice were implanted with the RhB degradation buffer solution for treatment. The body weights of mice increased during 21 days treatment (Fig. 7d). White blood cells (WBCs), red blood cells (RBCs), hemoglobin (HGB), hematocrit (HCT), and mean corpuscular hemoglobin (MCH) of the RhB solution groups exhibited obvious statistical differences with the control groups ($P < 0.01$, Table 1).

Compared to the control groups, most of the hematological results of RhB degradation filtrates exhibited no obvious statistical differences, except HCT ($P = 0.048$). Additionally, the blood chemical assay was performed. Alanine aminotransferase (ALT), aspartate aminotransferase (AST), albumin (ALB),

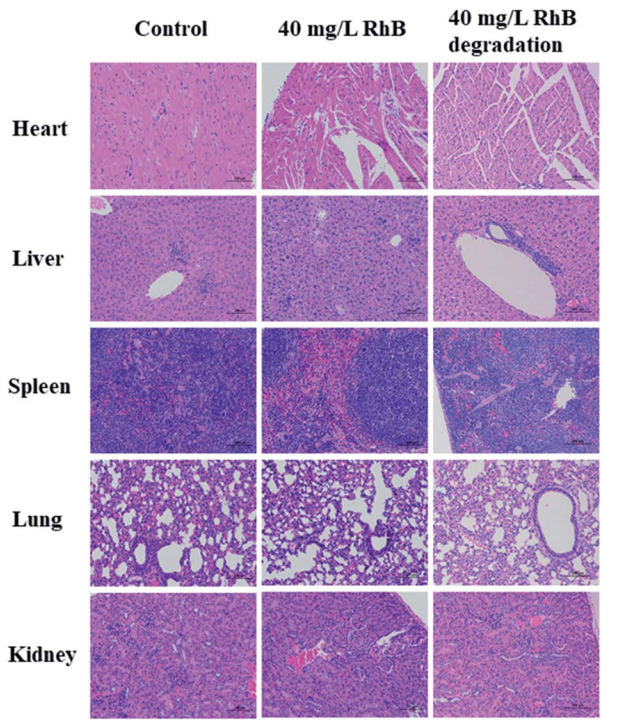

Fig. 8 H&E stained sections of the heart, liver, spleen, lung and kidney after 21 days treatment with the RhB degradation filtrate (substrate RhB concentration = 40 mg L^{-1}) or RhB solution (40 mg L^{-1}).

Table 2 Blood biochemistry analysis of mice after intravenous treatments with the RhB degradation filtrate (substrate RhB concentration = 40 mg L^{-1}) or RhB solution (40 mg L^{-1}) for 21 days[a]

Markers	Control group	RhB degradation filtrate	*P**	RhB solution	*P**
ALT[b]	45.95 ± 9.73	58.52 ± 11.33	0.053	91.39 ± 9.99	0.000
AST[b]	142.16 ± 16.16	149.91 ± 21.34	0.620	195.89 ± 37.31	0.003
ALB[b]	37.65 ± 4.57	41.08 ± 3.98	0.120	36.01 ± 1.43	0.442
ALP[b]	250.86 ± 78.84	234.66 ± 52.76	0.672	252.31 ± 60.32	0.970
TG[c]	0.96 ± 0.19	1.13 ± 0.23	0.313	1.11 ± 0.34	0.349
CHO[c]	2.19 ± 0.39	2.24 ± 0.50	0.856	2.29 ± 0.55	0.709
BUN[d]	6.11 ± 0.88	7.49 ± 1.58	0.077	6.70 ± 1.21	0.426
CREA[d]	25.24 ± 9.27	27.57 ± 3.57	0.226	14.71 ± 11.09	0.051
UA[d]	291.44 ± 97.01	324.36 ± 84.22	0.502	313.48 ± 64.09	0.652

[a] *P, compared with the control groups. [b] U L^{-1}. [c] mmol L^{-1}. [d] μmol L^{-1}.

alkaline phosphatase (ALP), triglycerides (TG) and total cholesterol (CHO) were the major biomarkers of liver function. The blood urea nitrogen (BUN) and creatinine (CREA) were related to kidney function. Also no obvious statistical differences were observed in RhB degradation filtrate groups. However, the ALT and AST of the RhB solution groups were greatly higher than those of the control groups ($P < 0.01$), which was associated with impaired liver function (Table 2). The pathological changes of major organs were compared with those of the control groups using the H&E staining assay (Fig. 8). The RhB solution groups showed high toxicity toward major organs. Hepatocytes with moderate degeneration were widely seen accompanied by a small amount of liver nuclear pyknosis. Occasional necrosis and nucleolysis were detected in liver cells. More aggregates of inflammatory cell infiltrates in liver lobules, lungs and kidneys were also seen. Yet the RhB degradation filtrate groups did not exhibit obvious pathological changes, compared to the controls. The toxicity of RhB degradation filtrates was assessed *in vitro* and *in vivo*, demonstrating that RhB degradation filtrates exhibited lower toxicity compared with those of RhB injection alone.

4. Conclusions

In this work, CuCDs were successfully prepared by a facile hydrothermal synthesis strategy. It was found that the addition of CuCDs helped the Fenton reaction accelerate RhB degradation in neutral solution. The catalytic activity of CuCDs was influenced by temperature, pH, concentration of CuCDs, metallic ions and electric charges. It was worth mentioning that electron transfer on the surface of CuCDs was found to be crucial in RhB degradation upon the Fenton reaction process as well as more $^{\cdot}OH$ and $^{1}O_2$ generation promoted by CuCDs. Moreover, the composition and microstructures of CuCDs had contributions to RhB degradation. The RhB degradation pathway was proposed on the basis of the results of LC-MS. Unlike other RhB degradation mechanisms, the strong oxidation of ROS caused the cleavage of the chromophore aromatic ring and the de-ethylation process in this work. In addition, the toxicity of RhB degradation filtrates was assessed *in vitro* and *in vivo*, demonstrating that the highly toxic RhB solution could convert to low-toxicity degradation products through the CuCD accelerated Fenton reaction. Therefore, CuCDs would be a promising Fenton catalyst to enhance the RhB degradation efficiency.

Conflicts of interest

There are no conflicts to declare.

Acknowledgements

This work was supported by the National Natural Science Foundation of China (81960558) and the Science Foundation of Guangxi Academy of Sciences (2018YJJ908).

References

1 Y. Liang, G. Huang, Q. Zhang, Y. Yang, J. Zhou and J. Cai, *J. Mol. Liq.*, 2021, **330**, 115580.
2 D. Joshy, S. Chakko, Y. A. Ismail and P. Periyat, *Nanoscale Adv.*, 2021, **3**(23), 6704–6718.
3 S. Mishra, L. Cheng and A. Maiti, *J. Environ. Chem. Eng.*, 2021, **9**(1), 104901.
4 S. Nayak, G. Swain and K. Parida, *ACS Appl. Mater. Interfaces*, 2019, **11**(23), 20923–20942.
5 S. Steplin Paul Selvin, A. Ganesh Kumar, L. Sarala, R. Rajaram, A. Sathiyan, J. Princy Merlin and I. Sharmila Lydia, *ACS Sustainable Chem. Eng.*, 2017, **6**(1), 258–267.
6 X. Li, J. Liu, A. I. Rykov, H. Han, C. Jin, X. Liu and J. Wang, *Appl. Catal., B*, 2015, **179**, 196–205.
7 M. Cheng, G. Zeng, D. Huang, C. Lai, P. Xu, C. Zhang and Y. Liu, *Chem. Eng. J.*, 2016, **284**, 582–598.
8 A. D. Bokare and W. Choi, *J. Hazard. Mater.*, 2014, **275**, 121–135.
9 X. Lai, X. A. Ning, J. Chen, Y. Li, Y. Zhang and Y. Yuan, *J. Hazard. Mater.*, 2020, **398**, 122826.
10 M. A. Tony and S. A. Mansour, *Nanoscale Adv.*, 2019, **1**(4), 1362–1371.
11 X. Huang, X. Hou, F. Jia, F. Song, J. Zhao and L. Zhang, *ACS Appl. Mater. Interfaces*, 2017, **9**(10), 8751–8758.
12 W. Meng, Y. Wang, Y. Zhang, C. Liu, Z. Wang, Z. Song, B. Xu, F. Qi and A. Ikhlaq, *J. Taiwan Inst. Chem. Eng.*, 2020, **111**, 162–169.
13 Y. Leng, W. Guo, X. Shi, Y. Li and L. Xing, *Ind. Eng. Chem. Res.*, 2013, **52**(38), 13607–13612.
14 Y. Cui, Z. Zhou, Y. Gao, L. Lei, J. Cao, R. Wu, L. Liang and Z. Huang, *J. Clean. Prod.*, 2021, **289**, 125807.
15 S. Ni, T. Zhou, H. Zhang, Y. Cao and P. Yang, *ACS Appl. Nano Mater.*, 2018, **1**(9), 5128–5141.
16 G. Huang, X. Chen, C. Wang, H. Zheng, Z. Huang, D. Chen and H. Xie, *RSC Adv.*, 2017, **7**(75), 47840–47847.
17 Q. Jiang, L. Liu, Q. Li, Y. Cao, D. Chen, Q. Du, X. Yang, D. Huang, R. Pei, X. Chen and G. Huang, *J. Nanobiotechnol.*, 2021, **19**(1), 64.
18 A. Sharma and J. Das, *J. Nanobiotechnol.*, 2019, **17**(1), 92–116.
19 J. Zhang, X. Liu, J. Zhou, X. Huang, D. Xie, J. Ni and C. Ni, *Nanoscale Adv.*, 2019, **1**(6), 2151–2156.
20 M. Pan, Z. Xu, Q. Jiang, J. Feng, J. Sun, F. Wang and X. Liu, *Nanoscale Adv.*, 2019, **1**(2), 765–771.
21 R. Wang, K. Q. Lu, Z. R. Tang and Y. J. Xu, *J. Mater. Chem. A*, 2017, **5**(8), 3717–3734.
22 V. Arul, T. N. Edison, Y. R. Lee and M. G. Sethuraman, *J. Photochem. Photobiol., B*, 2017, **168**, 142–148.
23 X. Xu, Z. Chen, Q. Li, D. Meng, H. Jiang, Y. Zhou, S. Feng and Y. Yang, *Microchem. J.*, 2021, **160**, 105708.
24 Y. Duan, Y. Huang, S. Chen, W. Zuo and B. Shi, *ACS Omega*, 2019, **4**(6), 9911–9917.
25 L. Lin, Y. Luo, P. Tsai, J. Wang and X. Chen, *Trac. Trends Anal. Chem.*, 2018, **103**, 87–101.
26 Z. X. Liu, B. B. Chen, M. L. Liu, H. Y. Zou and C. Z. Huang, *Green Chem.*, 2017, **19**(6), 1494–1498.

27 W. Wu, L. Zhan, W. Fan, J. Song, X. Li, Z. Li, R. Wang, J. Zhang, J. Zheng, M. Wu and H. Zeng, *Angew. Chem., Int. Ed.*, 2015, **54**(22), 6540–6544.
28 C. Han, X. Zhang, F. Wang, Q. Yu, F. Chen, D. Shen, Z. Yang, T. Wang, M. Jiang, T. Deng and C. Yu, *Carbon*, 2021, **183**, 789–808.
29 W. Qing, K. Chen, Y. Yang, Y. Wang and X. Liu, *Microchem. J.*, 2020, **152**, 104262.
30 P. P. Zhu, Z. Cheng, L. L. Du, Q. Chen and K. J. Tan, *Langmuir*, 2018, **34**(34), 9982–9989.
31 X. Ren, J. Liu, J. Ren, F. Tang and X. Meng, *Nanoscale*, 2015, **7**(46), 19641–19646.
32 J. Du, Y. Zhao, J. Chen, P. Zhang, L. Gao, M. Wang, C. Cao, W. Wen and C. Zhu, *RSC Adv.*, 2017, **7**(54), 33929–33936.
33 D. Yang, Q. Li, S. K. Tammina, Z. Gao and Y. Yang, *Sens. Actuators B Chem.*, 2020, **319**, 128273.
34 Z. Chai, C. Li, Y. Zhu, X. Song, M. Chen, Y. Yang, D. Chen, X. Liang and J. Wu, *Int. J. Bio. Macromol.*, 2020, **165**, 506–516.
35 X. Song, Z. Chai, Y. Zhu, C. Li and X. Liang, *Carbohydr. Polym.*, 2019, **219**, 316–327.
36 J. Guo, W. Lu, H. Zhang, Y. Meng, F. Du, S. Shuang and C. Dong, *Sens. Actuators B Chem.*, 2021, **330**, 129360.
37 N. Wang, W. Ma, Y. Du, Z. Ren, B. Han, L. Zhang, B. Sun, P. Xu and X. Han, *ACS Appl. Mater. Interfaces*, 2019, **11**(1), 1174–1184.
38 V. Lakshmi Prasanna and R. Vijayaraghavan, *J. Phys. Chem. C*, 2017, **121**(34), 18557–18563.
39 S. Pandiyan, L. Arumugam, S. P. Srirengan, R. Pitchan, P. Sevugan, K. Kannan, G. Pitchan, T. A. Hegde and V. Gandhirajan, *ACS Omega*, 2020, **5**(47), 30363–30372.
40 J. Xiao, J. Lai, R. Li, X. Fang, D. Zhang, P. Tsiakaras and Y. Wang, *Ind. Eng. Chem. Res.*, 2020, **59**(27), 12431–12440.
41 Z. Liang, M. Kang, G. F. Payne, X. Wang and R. Sun, *ACS Appl. Mater. Interfaces*, 2016, **8**(27), 17478–17488.
42 D. F. Eaton, *Pure Appl. Chem.*, 1988, **60**(7), 1107–1114.
43 B. Sun, H. Li, X. Li, X. Liu, C. Zhang, H. Xu and X. S. Zhao, *Ind. Eng. Chem. Res.*, 2018, **57**(42), 14011–14021.
44 H. Yin, D. Gao, Y. Qiu, G. Yi, J. Li, Y. Dong, K. Zhang, Z. Xia and Q. Fu, *Nanoscale Adv.*, 2020, **2**(4), 1483–1492.
45 N. Dhenadhayalan, K. C. Lin and T. A. Saleh, *Small*, 2020, **16**(1), 1905767.
46 B. Palanivel and A. Mani, *ACS Omega*, 2020, **5**(31), 19747–19759.
47 W. Yu, T. Liu, M. Zhang, Z. Wang, J. Ye, C. X. Li, W. Liu, R. Li, J. Feng and X. Z. Zhang, *ACS Nano*, 2019, **13**(2), 1784–1794.
48 S. Sahar, A. Zeb, C. Ling, A. Raja, G. Wang, N. Ullah, X. M. Lin and A. W. Xu, *ACS Nano*, 2020, **14**(3), 3017–3031.
49 Y. J. Chung, B. I. Lee, J. W. Ko and C. B. Park, *Adv. Healthc. Mater.*, 2016, **5**(13), 1560–1565.
50 B. Wang, G. Zhang, Z. Sun, S. Zheng and R. L. Frost, *J. Environ. Chem. Eng.*, 2015, **3**(3), 1444–1451.